TiPS

Evaluation of the inhibitory activities of thyme compounds against coronavirus disease-19 (COVID-19) by molecular docking and molecular dynamic simulation

Saba Hadidi*

Inorganic Chemistry Department, Faculty of Chemistry, Razi University, Kermanshah, Iran

Abstract

We have explored the inhibitory capability of *Thymus vulgaris* compounds against ACE2 protein -the host receptor for SARS-CoV-2, papain-like and main protease of the SARS-CoV-2 through molecular simulations. The docking results showed that the compounds had a greater capability to inhibit ACE2 and papain-like protease in comparison to the main protease. The majority of compounds (61.7%) bind to the S2 active pocket of ACE2. The most powerful anticoronavirus activity is expressed in the order: Terpinolene > Thymol > Bicyclogermacrene. Pi interactions play key roles in the binding of three compounds to the active sites of ACE2 enzyme. 34 out of these 60 compounds were fitted in the PLpro active site. α-humulene followed by (+)-Spathulenol, and (-)-β-Bourbonene showed strong capacity to inhibit PLpro binding site. Except for (+)-Spathulenol which also formed H-bond with Asp165 and Tyr274 amino acids, α-humulene and (-)-β-Bourbonene conjugate with PLpro were stabilized mainly through alkyl and pi interactions. According to the Mpro docking results, 58.3% of thyme compounds could block the active site. The binding energy order was (-)-Spathulenol at highest, then Bicyclogermacrene, (+)-δ-cadinene, (+)-Spathulenol, and Viridiflorol, followed by (-)-β-Caryophyllene oxide. Cys145, His41, Met49, and Met165 are key residues in the interaction of these ligands with the enzyme binding site. The weakest interaction with all three enzymes was observed for (R)-(-)-1-Octen-3-ol and (3S)-Oct-1-en-3-ol. Based on the molecular dynamics simulation lowest conformational change was detected for ACE2 in the present of Terpinolene. (-)-Spathulenol and α-Humulene had the least and most displacement compared to its initial positions, respectively.

Keywords: Covid-19, Thyme compounds, Molecular modeling

1. Introduction

The SARS CoV-2 pandemic is one of the most dangerous infectious diseases which cause considerable threat to human health worldwide (1). Nowadays, this illness draws the attention of many researchers as a global health crisis at individual and public health levels. A huge number of scientists are currently trying to find effective solutions and methods to detect, prevent and cure SARS-CoV-2. Using Plant essential oils and medicine derived from natural herbs are two suitable ways for treatment of various diseases (2, 3). *Thymus vulgaris* (thyme) is a Mediterranean aromatic of the Labiatae family (4), which can be used for medicinal purposes due to its properties such as, antimicrobial, anthelmintic, antibroncholitic, antispasmodic, sedative, diaphoretic, carminative,

Corresponding Author: Saba Hadidi, Inorganic Chemistry Department, Faculty of Chemistry, Razi University, Kermanshah, Iran
Email: s.hadidi@razi.ac.ir

Saba Hadidi.

antitussive, and diuretic properties (5-8). *Thymus vulgaris* is commonly utilized in folk medicine in the treatments of several kinds of diseases including, bronchopulmonary disorders, respiratory tract infections, gastroenteric, laryngitis, and inflammation (4, 9-11). This herb can be effective in cases of assorted intestinal infections and infestations, like gram-negative and gram-positive bacterium. Several studies confirmed anti-microbial activities of *Thymus vulgaris* against different bacterial species such as *Helicobacter pylori*, *Staphylococcus aureus*, and *Salmonella typhimurium* (12-15). The obtained results indicated that *Thymus vulgaris* plays a significant role in stopping the growth of the microorganism species examined (16, 17). It has been reported that the flavonoids in thyme is able to relax tracheal and ileal smooth muscles (18, 19). The thyme extract and volatile oil can relax tracheal and ileal smooth muscles by inhibiting phasic contractions and through β2-receptors (20-22). Moreover, this herb can act as an appetite stimulant and improve liver functioning (17). The antioxidant properties of thyme oil can be attributed to a biphenyl compound and a flavonoid isolated from thyme which is capable of protecting red blood cells against oxidative damage via inhibition of superoxide anion production (23-26). A group of researchers confirmed the antiviral activity of *Thymus vulgaris* against *Herpes simplex* virus. The experimental results depicted that this herb is able to inhibit the growth of *Herpes simplex* virus type 1 (HSV-1), type 2 (HSV-2) and an acyclovir-resistant strain of HSV-1 (27). Furthermore, it has been reported that drinking infusions or decoctions of Medicinal plants such as *Thymus vulgaris* and *Eucalyptus aerial* parts have a crucial role in treatment of respiratory tract infections (28-32). Various species of *Thymus* can be found in many countries which are different in type of components and content. However, normally they contain flavonoids, thyme, carvacrol, and phenol compounds (33). The study aimed to evaluate the ability of *Thymus vulgaris* components in inhibiting Angiotensin-converting enzyme 2 (ACE2) protein in human body. In this process *Thymus vulgaris* causes SARS-CoV-2 to lose its host receptor and destroy its protein (Covid-19 main protease). It is noteworthy to note that the ACE2 protein is the host receptor of the SARS-CoV-2 and SARS-CoV (34-36). The significant point is that if the ACE2 protein can be inhibited by *Thymus vulgaris* components, the SARS-CoV-2 could be prevented and cured. In this investigation we used molecular docking and molecular dynamic simulations to predict and determine the capability of these components to inhibit ACE2 protein in human body as weel as papain-like protease and main protease of SARS-CoV-2.

2. Material and methods
2.1. Molecular docking simulation
The 3D structures of 60 compounds of thyme as ligands were obtained in .mol format from ChemSpider database (http://www.chemspider.com) (37) and converted into .pdb format through BIOVIA Discovery Studio Visualizer 2016 (38). The structures were optimized with semi-empirical PM6 method using ORCA software (39). Crystal structures of the SARS-CoV-2 main protease (PDB ID: 6LU7), papain-like protease (PDB ID: 5Y3e), and human entry receptor ACE2 (PDB ID: 1R42) were downloaded from RCSB PDB database (http://www.rcsb.org/pdb) (40). Before docking calculation, the enzymes were edited by removing the solvent molecules, ions, and unnecessary protein chains. The polar hydrogen atoms and Gasteiger charges were included in the receptor structure and then the protein in PDBQT format was used as an input for the AutoDock Vina program (41). The remaining parameters were set as default. For each target protein, the specific grid size (x, y, and z) points, and the grid center (x, y, and z dimensions) were set with a grid spacing of 1 Å to cover the active site residues. For each of the docking cases, the best energy docked conformation was extracted from the 20 minimum energy conformers from the 500 runs and the binding affinity was determined through kcal/mol. BIOVIA Discovery Studio Visualizer 2021 and LigPlot+ (42) were visualized to post-docking analysis of output, giving details of the locations of binding sites, hydrogen, and hydrophobic interactions of the docked ligand in various confirmations.

2.2. Molecular dynamic simulation
The molecular dynamics (MD) simulation

Table 1. Active sites residues of ACE2 enzyme.	
Binding site	Residues
S1 pocket	Arg273, Phe274, Pro346, Asp367, Leu370, Thr371, His374, Glu375, Glu402, Glu406, Ser409, Leu410, Ala413, Phe438, Gln442, Thr445, Ile446, Thr449, Thr453, Phe512, Tyr515, Arg518, Thr519, Gln522
S2 pocket	Phe340, Pro346, Thr347, Ala348, Asp350, Gly352, His374, Glu375, His378, Asp382, Tyr385, Phe390, Arg393, Asn394, His401, Glu402

was carried out for the most promising compounds Terpinolene, α-Humulene, and (-)-Spathulenol against ACE2, PLpro, and Mpro, respectively, using Groningen Machine for Chemical Simulation (GROMACS) version 2020.2. Topology parameter for protein was generated With amber99sb force field and ligands topology was obtained from the Winmostar software. The protein-ligand system was embedded into a cubic box of 10 Å dimension using SPCE water model. The overall system was neutralized by adding Na^+ or Cl^- ions (0.15 M). An initial minimization was performed for 100 ps in two phases i.e. (canonical) NVT equilibration and (thermal-isobaric) NPT equilibration at a uniform temperature and pressure of 310 K and 1 bar. Once ready, the systems were simulated for 50 ns in NPT ensemble and the trajectories were calculated with a time step of 2 fs and snapshots were saved at every 50 ps. The structural behaviour of receptors in the absence and presence of the ligand molecules were investigated through Root mean square deviation (RMSD) and Root mean square fluctuation (RMSF).

3. Result and discussion

### 3.1. Molecular docking simulations into ACE2 active sites

Angiotensin-converting enzyme 2 (ACE2) is a protein-coding gene on the surface of many cell and tissue types in human body, including lungs, arteries, heart, kidney, and intestines, but in different quantities (43). Unlike children, a high concentration of ACE2 enzyme was observed in patients with hypertension, diabetes, and coronary heart diseases (44-46). Studies have found that ACE2 acts as a human host receptor for the SARS-CoV-2, thus, if the ACE2 active site is blocked, the virus entering to the human cells can be prevented (47). To this aim, molecular docking simulation was used to evaluate the inhibitory activity

of thyme compounds against S1 and S2 binding pockets of ACE2 (Table 1).

A summary of the obtained results including the binding energy, binding site, interaction force, as well as interaction distance between 60 ligands and amino acids in ACE2 active sites are available in the Supporting Information (Table S1). The majority of compounds (61.7%) showed inhibitory activity against S2 pocket with binding energy in the range of -4.2 to -6.7 kcal/mol, while compounds that bind to S1 pocket had higher binding affinity (-4.5 to -7.0 kcal/mol). Terpinolene, Thymol, and Bicyclogermacrene exhibited the best potential inhibitors toward S1 and S2 pocket, respectively, while (R)-(-)-1-Octen-3-ol showed the lowest docking score (-4.2 kcal/mol) followed by (3S)-Oct-1-en-3-ol (-4.5 kcal/mol), and Geraniol (-4.7 kcal/mol) (Table S1). The inhibitory activity of Terpinolene that shows the highest binding affinity (-7.0 kcal/mol) is attributed to hydrophobic type interactions with Phe438 as one of the key residue at S1 active pocket. Three pi-alkyl and one pi-sigma interactions were formed between the aromatic side chain of Phe438 with C atoms of methyl group, isopropyl substituent, and C6 of cyclohexene ring, respectively (Figure 1).

Similar to Terpinolene, Thymol interacts with Phe438 at S1 binding pocket, but with a small difference in binding energy (-6.8 kcal/mol). The aromatic side chain of Phe amino acid is positioned over the ligand molecule, making two pi-alkyl and a pi-pi stacking interactions with C atoms of methyl and isopropyl groups as well as benzene aromatic ring in Thymol, respectively (Figure 2). Also thymol hydrophobically interacts with Ala413 (Table S1).

The main interactions of Bicyclogermacrene with amino acids in S2 pocket of ACE2 enzyme are Asp350, Asp382, Tyr385, Phe390, Arg393, and, Asn394 with binding affinity -6.7
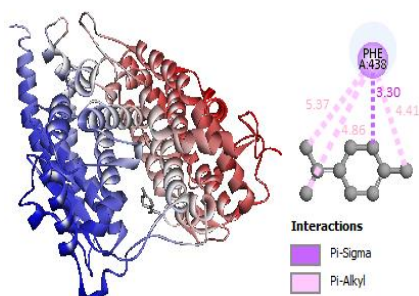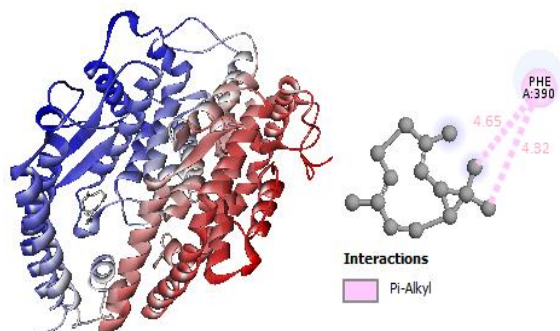
Figure 1. Terpinolene docked into ACE2 enzyme (left) and amino acid residue involved in the interaction (right), the dashed line shows type of interaction and distance in Å.

kcal/mol (Table S1). Conformational stability of the ligand-protein complex is maintained by hydrophobic interactions. As shown in Figure 3, two pi-alkyl bonds, a type of hydrophobic interaction, were formed between methyl groups attached to cyclopropane ring and benzene ring in Phe390.

3.2. Molecular docking simulations into papain-like protease active site

The papain-like cysteine protease (PLpro) is an essential coronavirus enzyme that plays a key role in the virus replication cycle. This process is initiated by the synthesis of pp1a/pp1ab polyproteins that are translated from ORF1a/ORF1b of the virus genome. Cleavage of these poly-proteins release virus non-structural proteins which orchestrate viral replication (48). PLpro is also implicated in cleaving proteinaceous post-translational modifications on host proteins as an evasion mechanism against host antiviral immune responses (49). Targeting PLpro by antiviral agents may inhibit both viral replication and the dysregulation of signaling cascades in infected cells which lead
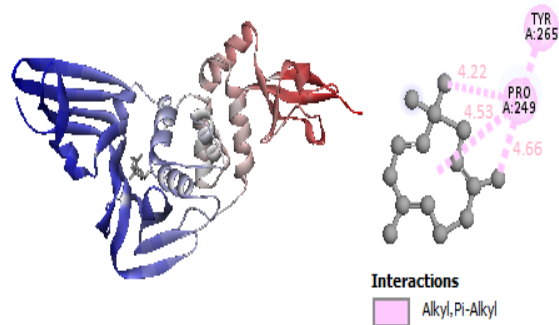

Figure 3. Bicyclogermacrene docked into ACE2 enzyme (left) and amino acid residue involved in the interaction (right) the dashed line shows type of interaction and distance in Å.
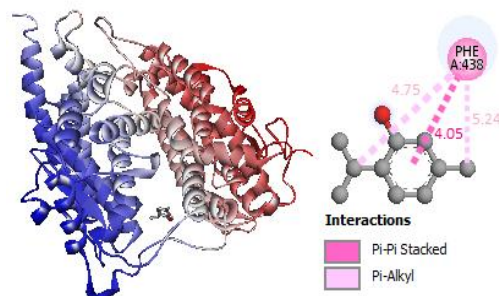
Figure 2. Thymol docked into ACE2 enzyme (left) and amino acid residue involved in the interaction (right) the dashed line shows type of interaction and distance in Å.

to cell death in surrounding, uninfected cells (50). In this viewpoint, thyme compounds were docked into PLpro active site (Pro248, Pro249, Tyr269, Asp165, Glu168, Leu163, Gly164, Gln270, Tyr274, Tyr265, and Thr302) for developing potential antiviral agents directed against this promising target. The results indicate that 34 out of these 60 compounds were fitted in the active site with a docking score of -4.5 to -7.1 kcal/mol (Table S2). Best among them that show strong binding in the pocket of enzyme are α-Humulene (-7.1 kcal/mol) followed by (+)-Spathulenol (-7.0 kcal/mol), and (-)-β-Bourbonene (-6.9 kcal/mol).

The results illustrate that Asp165, Pro249, Tyr265, Tyr269, Tyr274, and Thr302 are key residues in the interaction of α-Humulene with enzyme binding site (Table S2). The 2D diagram of α-Humulene binding to PLpro active pocket showing a pi-alkyl interaction between Tyr265 and methyl group attached to C9 of bicycle ring at distance 4.66 Å and two alkyl interactions between Pro249 and -CH$_3$ branch attached to C6 and aromatic center of C ring with a bond length of 4.22

Figure 4. α-Humulene docked into PLpro enzyme (left) and amino acid residues involved in the interaction (right) the dashed line shows type of interaction and distance in Å.
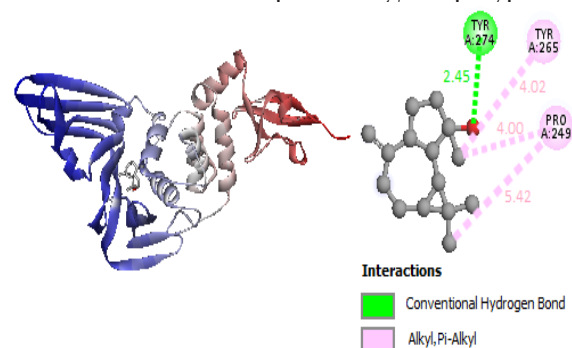
and 4.53 Å, respectively (Figure 4).

(+)-Spathulenol, second highest and very close binding score to α-Humulene, bind through three different interactions with Asp165, Pro249, Tyr265, and Tyr274 main residues (Table S2). One O-H···O type hydrogen bond with distance of 2.45 Å formed between the oxygen of the carboxyl group of ligand and the hydrogen of the hydroxyl group in Tyr274 residue. It also forms alkyl interactions between, Pro249-C of methyl substituent at position 7 and Pro249-C of methyl substituent at position 1 with a bond length of 4.00 and 5.42 Å, respectively. Docking pose of (+)-Spathulenol displayed a pi-alkyl interaction with Tyr265 and C of methyl substituent at position 7 at distance 4.02 Å (Figure 5).

Figure 6 shows the docking pose for (-)-β-Bourbonene and the interacting amino acid residues in PLpro active site. From Figure 6, it can be seen that (-)-β-Bourbonene interacts with two amino acids by three types of interactions. These are: two alkyl interactions between Pro249 with –CH$_3$ attached to cyclobutane ring and the center of cyclopentane ring at distances of 4.39 and 5.37 Å, respectively, two pi-alkyl and one pi-sigma interaction between Tyr265 and the center of cyclopentane ring, isopropyl and methyl groups attached to cyclobutane ring with a bond length 4.75, 5.19, and 3.69 Å, respectively.

3.3. Molecular docking simulations into main protease active site

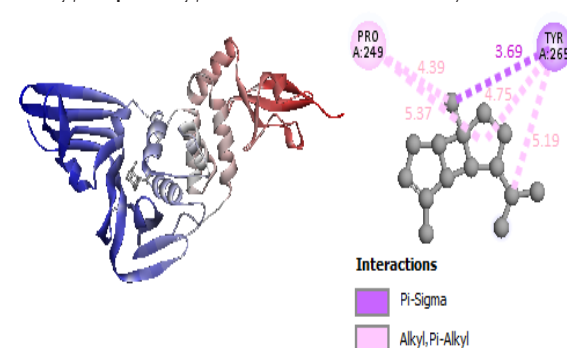The main protease (Mpro, also named 3CLpro) is one of the promising drug targets due to its essential role in processing the polyproteins that are translated from the viral RNA (51). The active site of Mpro is located in the gap between domains I (residues 8-101) and II (residues 102-184), which contains a CysHis catalytic dyad (Cys145 and His41) (52). The Cys residue is responsible for Michael addition reaction and nucleophilic attack in biological processes (53).

The Mpro docking results showed that 35 of the 60 thyme compounds (58.3%) were located in the binding site with energies ranging from -3.7 kcal/mol to -5.6 kcal/mol. (Table S3). We found that the binding energy order was (-)-Spathulenol at highest, then Bicyclogermacrene, (+)-δ-cadinene, (+)-Spathulenol, and Viridiflorol, followed by (-)-β-Caryophyllene oxide with a slight difference. The interaction between (-)-Spathulenol with the receptor binding site was stabilized by a conventional hydrogen bond between –OH group of ligand with carbonyl group of Glu166 residue with a bond length 2.28 Å, two pi-alkyl interactions between His41 with cycloheptane ring and attached –CH$_3$ group at distances 4.41 and 5.05 Å, respectively, and alkyl interactions between Cys145-C of –CH$_3$ group attached to cyclopropane ring, Met49 with the center of cycloheptane ring, and Met165 with –CH$_3$ group at position 4 with a range of 4.02 to 5.44 Å (Figure 7).

Bicyclogermacrene, (+)-δ-cadinene, (+)-Spathulenol, and Viridiflorol were fitted in the Mpro active pocket with similar binding energy (-5.5 kcal/mol). From Figure 8, it is apparent that two H-bonds formed, one between O atom of hydroxyl group in Viridiflorol and H atom of –NH group in His163 and another one between H of –OH group in ligand with S atom of Cys145 with a

Figure 5. (+)-Spathulenol docked into PLpro enzyme (left) and amino acid residues involved in the interaction (right) the dashed line shows type of interaction and distance in Å.

Figure 6. (-)-β-Bourbonene docked into PLpro enzyme (left) and amino acid residues involved in the interaction (right) the dashed line shows type of interaction and distance in Å.
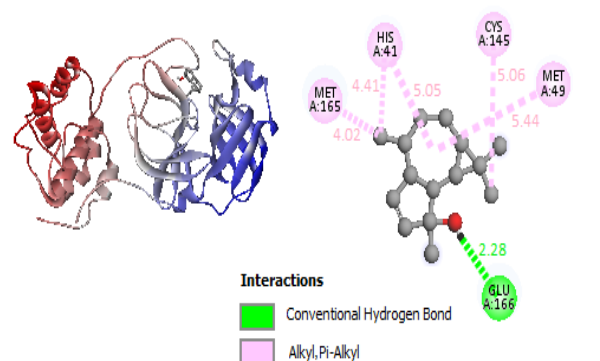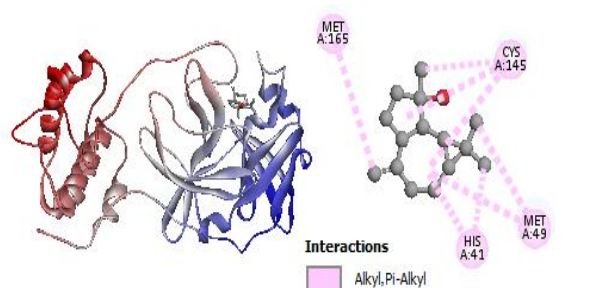
Figure 7. (-)-Spathulenol docked into Mpro enzyme (left) and amino acid residues involved in the interaction (right) the dashed line shows type of interaction and distance in Å.
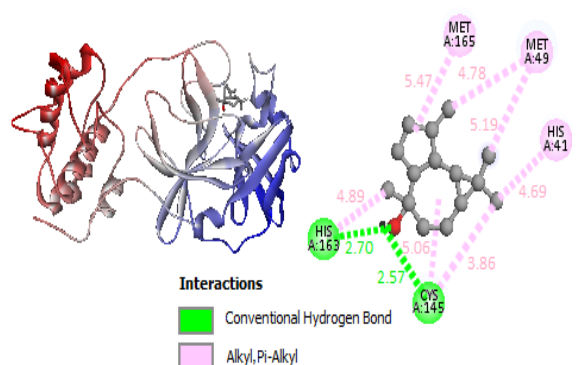
bond length 2.70 and 2.57 Å, respectively. Moreover, alkyl interactions between Viridiflorol and receptor amino acids Cys145, Met165, and Met49 along with pi-alkyl interactions with His163 and His41 played key roles in stabilizing the ligand-receptor conjugate.

The interaction of (+)-Spathulenol with the Mpro was seen in alkyl interactions; one between Met165 and –CH$_3$ group attached to cycloheptane ring, two between Met49 with the carbon center of cycloheptane ring and methyl substituent of cyclopropane ring, and three between Cys145 with cycloheptane ring, the center and –CH$_3$ group of cyclopentane ring. Also two pi-alkyl interactions were observed between His41 with cycloheptane ring and –CH$_3$ group attached to cyclopropane ring (Figure 9).

The major interaction between (+)-δ-cadinene and the protease was characterized by two alkyl interactions between Met49 and C of methyl substituent at position 4 at distance 3.68 Å and Met165 with the center of C ring with a bond length 4.91 Å. Also, a pi-alkyl interaction

Figure 8. Viridiflorol docked into Mpro enzyme (left) and amino acid residues involved in the interaction (right) the dashed line shows type of interaction and distance in Å.
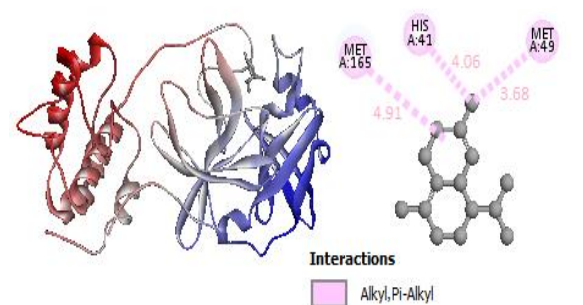
of methyl substituent at position 4 and His41 was observed (Figure 10).

Bicyclogermacrene is surrounded by Leu141, Asn142, Met49, His41, and Cys145 amino acids in the Mpro active site. 4 alkyl interactions between Cys145 and 3 methyl substituents as well as the center of bicyclo ring at distance 3.95 to 5.44 Å were characterized in the ligand-receptor complex (Figure 11).

(-)-β-Caryophyllene oxide docked in the covid-19 Mpro yielding a binding affinity of -5.3 kcal/mol. Significant binding was observed, with 5 alkyl interactions between both methyl substituents, the center of bicyclo and cyclobutane ring of ligand with Cys145 as well as between C atom of =CH$_2$ group and Met49 residue. Also two pi-alkyl interactions were characterized between the center of ring of His41 with C atom of =CH$_2$ group and the cyclobutane ring (Figure 12).

3.4. Molecular dynamic simulations

Among the ligands screened through

Figure 9. (+)-Spathulenol docked into Mpro enzyme (left) and amino acid residues involved in the interaction (right).

Figure 10. (+)-δ-cadinene docked into Mpro enzyme (left) and amino acid residues involved in the interaction (right) the dashed line shows type of interaction and distance in Å.
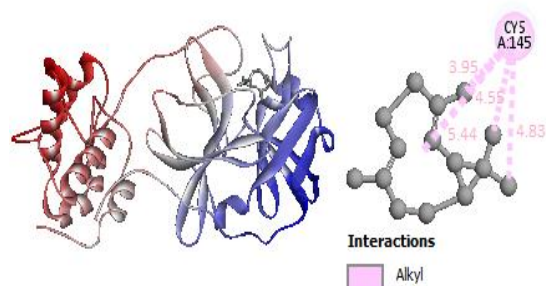
Figure 11. Bicyclogermacrene docked into Mpro enzyme (left) and amino acid residues involved in the interaction (right) the dashed line shows type of interaction and distance in Å.

docking studies, Terpinolene, α-Humulene, and (-)-Spathulenol revealed high binding affinities to ACE2, PLpro, and Mpro, respectively. Therefore, these compounds were selected as the most effective inhibitors and used for further analysis using MD simulations. The RMSD values of back bone atoms in proteins and protein-ligand complexes were calculated to investigate the protein structure variation by ligand molecule. It was observed that all simulations were stable as indicated by RMSD plots (Figures 13A, B, and C). The ACE2, PLpro, and Mpro showed an average RMSD of 1.64, 1.69, and 2.39 Å, which increased to 1.67, 2.73, and 3.39 in the present of Terpinolene, α-Humulene, and (-)-Spathulenol, respectively. The least conformational change was detected for a complex of ACE2 with Terpinolene.

A Larg deviation was obtained for a trajectory segment between about 17 and 37 ns, but after 37 ns of simulation Terpinolene's RMSD was stabilized with an average of 0.47 Å (Figure 13A). As can be seen from Table 2, the Terpinolene's binding position was stabilized after 25 ns with 46% similarity in the binding site residues, in which Ala413, Gln442, and Phe438 were seen as main residues at S1 binding pocket of ACE2 in ligand-protein complex (Figure 14). These observations are in good agreement with the molecular docking results presented in Figure 1.

With 12.5% similarity in the amino acids of the binding site, α-Humulene had the most displacement compared to its initial position (Table 3). Glu168 is the only amino acid from the active site of PLpro that interacts with ligand by the van der Waals force (Figure 15).

(-)-Spathulenol showed to be stable inside
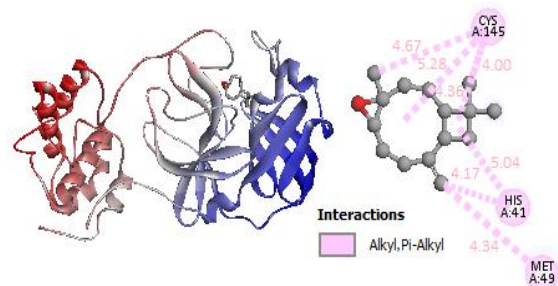
Figure 12. (-)-β-Caryophyllene oxide docked into Mpro enzyme (left) and amino acid residues involved in the interaction (right) the dashed line shows type of interaction and distance in Å.

the binding pocket during all 50 ns simulation with very low value of ligand's RMSD 0.26 Å (Figure 13C) and high percentage of binding site residues similarity (Table 4). A comparison between Figure 7 and Figure 16 had clearly shown that His41, Met49, and Met165 were main residues in
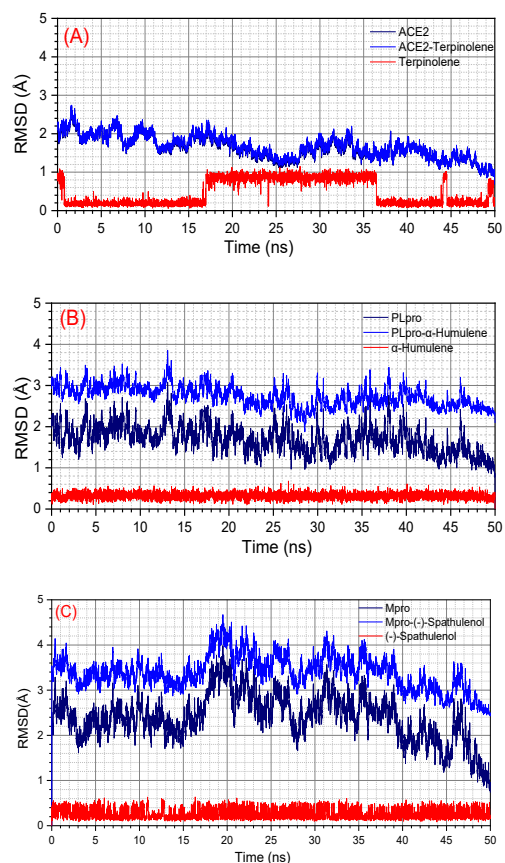
Figure 13. Plots of Root Mean Square Deviation (RMSD) values for the backbone atoms of protein (black), protein-ligand complex (blue), and ligand (red) from initial structures throughout the 50 ns simulation as a function of time. (A) ACE2, (B) PLpro, and (C) Mpro.
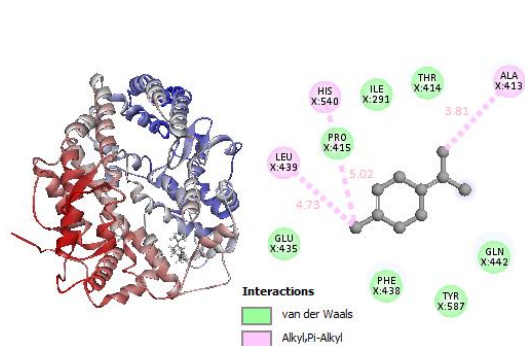
Figure 14. Binding position and principal interactions of Terpinolene with ACE2 peptide observed at time 50 ns of MD simulation trajectories.

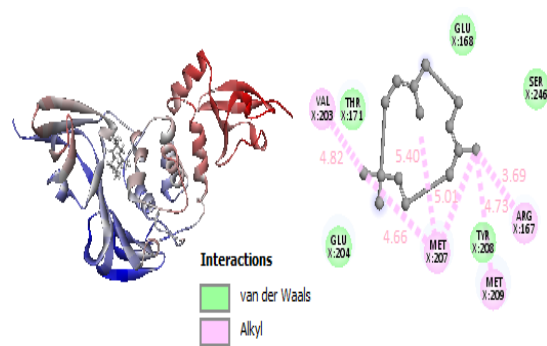Figure 15. Binding position and principal interactions of α-Humulene with PLpro peptide observed at time 50 ns of MD simulation trajectories.

Table 2. Residues involve in Terpinolene-ACE2 complex at different simulation times.

Time (ns)	% Binding site residues similarity	% Binding site residues similarity
	Residues involve in interaction	(Relative to the initial position)
0	Tyr279, Lys288, Pro289, Asn290, Ile291, Ala413, Thr414, Pro415, Phe428, Thr434, Asn437, Phe438, Gln442, His540, Lys541	100
10	Ile291, Leu410, Ala413, Thr414, Pro415, Thr434, Glu435, Phe438, Leu439, His540, Lys541, Tyr587	53.3
25	Ala413, Thr414, Pro415, Lys416, Glu435, Phe438, Leu439, Gln442, His540, Lys541, Cys542, Asp543, Tyr587	46.6
50	Ile291, Ala413, Thr414, Pro415, Glu435, Phe438, Leu439, Gln442, His540, Tyr587	46.6

(-)-Spathulenol-Mpro interaction process.

The residue-based root mean square fluctuation (RMSF) in the trajectory was calculated to examine the flexibility of the peptide structure. Higher RMSF values show greater flexibility during the MD simulation. The RMSF result for ACE2 with 596 amino acids shows the average value of 11.95 Å, which indicates the low flexibility of amino acids, except for Ile119 with RMSF 21.29 Å (Figure 17A). Close observation of the PLpro RMSF plot analysis confirmed that the fluctuations balance at the beginning of the peptide is less compared to the end. Also, the α-Humulene interaction with Arg167, Glu168, Thr171, Val203, Glu204, Met207, Tyr208, Met209, and Ser246 amino acids leds to a reduction in their fluctuation (Figure 17B). The RMSF result for Mpro with 305

amino acids is plotted in Figure 17C, which shown that the fluctuations balance at the middle (residues from about 60 to 140) and end (residues from about 200 to 305) of the peptide is greater and in the the beginning (residues from about 30 to 55) and the middle (residues from about 160 to 200) region in effect of binding of (-)-Spathulenol with the peptide, the flexibility amount of the residues is reduced.

4. Conclusion

In conclusion, the current study used molecular docking and molecular dynamic simulation analysis to explore 60 substances in *Thymus vulgaris* against the structural targets of SARS-CoV-2 (PLpro and Mpro) and human ACE2 receptor for the prevention and treatment of COVID19 infec-

Table 3. Residues involve in α-Humulene-PLpro complex at different simulation times.

| Time	α-Humulene-PLpro	% Binding site residues similarity
	Residues involve in interaction	(Relative to the initial position)
0 ns	Met209, Pro248, Pro249, Tyr265, Asn268, Tyr269, Tyr274, Thr302	100
50 ns	Arg167, Glu168, Thr171, Val203, Glu204, Met207, Thr208, Met209, Ser246	12.5

Table 4. Residues involve in (-)-Spathulenol-Mpro complex at different simulation times.

Time	(-)-Spathulenol-Mpro	% Binding site residues similarity
	Residues involve in interaction	(Relative to the initial position)
0 ns	His41, Met49, Gly143, Cys145, His164, Met165, Glu166, Val186, Asp187, Arg188, Gln189	100
50 ns	Thr25, His41, Cys44, Met49, Pro52, Tyr54, His164, Met165, Val186, Asp187, Arg188, Gln189, Gln192	72.7
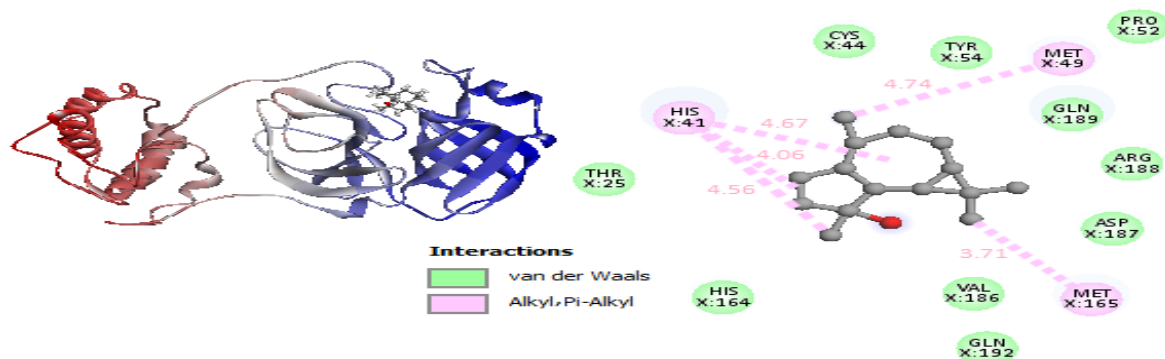
Figure 16. Binding position and principal interactions of (-)-Spathulenol with Mpro peptide observed at time 50 ns of MD simulation trajectories.

tion. The top candidates were identified based on binding position, binding affinity, interaction force and other parameters that explain their ability to inhibit SARS-CoV-2. In contrast to Mpro, the compounds were found to be more effective at inhibiting ACE2 and PLpro. Terpinolene, α-Humulene, and (-)-Spathulenol showed strong affinities for ACE2, PLpro, and Mpro, respectively. Hydrophobic force including pi-sigma and pi-alkyl interactions play key roles in Terpinolene–ACE2 binding process. Unlike (-)-spathulenol binding to Mpro, where hydrogen bonds contribute to the stabilization of the ligand-receptor complex in addition to hydrophobic interactions, α-Humulene interacts with PLpro only by alkyl and pi-alkyl interactions. (R)-(-)-1-Octen-3-ol and (3S)-Oct-1-en-3-ol had the lowest interactions with all three enzymes. MD simulations showed that the least conformational changes in the receptor were related to the ACE2 in the presence of Terpinolene. α-Humulene shifted the most from its initial position, while (-)-Spathulenol was stable inside the binding pocket during all 50 ns simulation. This study brings out a recommendation to use *Thymus vulgaris* in preventing infections and limiting the spread of SARS-CoV-2. However, preclinical studies should perform on molecular mechanism to establish the possible relationship of the results obtained in this
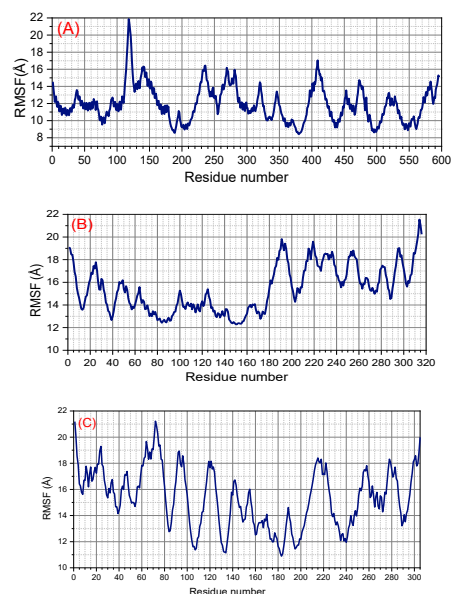
Figure 17. Root mean square fluctuation (RMSF) of the backbone atoms of (A) ACE2 in complex with Terpinolene, (B) α-Humulene-PLpro complex, and (C) (-)-Spathulenol-Mpro conjugate during 50 ns of molecular dynamics simulations.

research with the observed biological activity of this natural compound on SARS-CoV-2.

Conflict of Interest

None declared

Saba Hadidi.

References

1. Chen J. Pathogenicity and transmissibility of 2019-nCoV-A quick overview and comparison with other emerging viruses. *Microbes Infect*. 2020 Mar;22(2):69-71. doi: 10.1016/j.micinf.2020.01.004. Epub 2020 Feb 4. PMID: 32032682; PMCID: PMC7102641.

2. Lis-Balchin M, Deans SG. Bioactivity of selected plant essential oils against Listeria monocytogenes. *J Appl Microbiol*. 1997 Jun;82(6):759-62. doi: 10.1046/j.1365-2672.1997.00153.x. PMID: 9202441.

3. Janssen AM, Scheffer JJ, Baerheim Svendsen A. Antimicrobial activities of essential oils. A 1976-1986 literature review on possible applications. *Pharm Weekbl Sci*. 1987 Aug 21;9(4):193-7. doi: 10.1007/BF02029329. PMID: 3309882.

4. Ocaña A, Reglero G. Effects of Thyme Extract Oils (from Thymus vulgaris, Thymus zygis, and Thymus hyemalis) on Cytokine Production and Gene Expression of oxLDL-Stimulated THP-1-Macrophages. *J Obes*. 2012;2012:104706. doi: 10.1155/2012/104706. Epub 2012 Apr 17. PMID: 22577523; PMCID: PMC3345235.

5. Sáez F, Stahl-Biskup E. Essential oil polymorphism in the genus Thymus. Thyme–the genus Thymus. London: Taylor & Francis. 2002; 125-43.

6. Cruz T, Cabo MP, Cabo MM, Jimenez J, Cabo J, Ruiz C. In vitro antibacterial effect of the essential oil of Thymus longiflorus Boiss. *Microbios*. 1989;60(242):59-61. PMID: 2514339.

7. Rota C, Carramiñana JJ, Burillo J, Herrera A. In vitro antimicrobial activity of essential oils from aromatic plants against selected foodborne pathogens. *J Food Prot*. 2004 Jun;67(6):1252-6. doi: 10.4315/0362-028x-67.6.1252. PMID: 15222560.

8. Mărculescu A, Vlase L, Hanganu D, Drăgulescu C, Antonie I, Neli-Kinga O. Polyphenols analyses from Thymus species. *J Proc Rom Acad Series B*. 2007;3:117-21.

9. Rustaiyan A, Masoudi S, Monfared A, Kamalinejad M, Lajevardi T, Sedaghat S, Yari M. Volatile constituents of three Thymus species grown wild in Iran. *Planta Med*. 2000 Mar;66(2):197-8. doi: 10.1055/s-0029-1243136. PMID: 10763607.

10. Taylor L. Plant based drugs and medicines. *Raintree Nutrition Inc*. 2000; 1-5.

11. Nickavar B, Mojab F, Dolat-Abadi R. Analysis of the essential oils of two Thymus species from Iran. *Food Chem*. 2005;90:609-11. doi.org/10.1016/j.foodchem.2004.04.020

12. Agnihotri S, Vaidya AD. A novel approach to study antibacterial properties of volatile components of selected Indian medicinal herbs. *Indian J Exp Biol*. 1996 Jul;34(7):712-5. PMID: 8979514.

13. Juven BJ, Kanner J, Schved F, Weisslowicz H. Factors that interact with the antibacterial action of thyme essential oil and its active constituents. *J Appl Bacteriol*. 1994 Jun;76(6):626-31. doi: 10.1111/j.1365-2672.1994.tb01661.x. PMID: 8027009.

14. Manou I, Bouillard L, Devleeschouwer MJ, Barel AO. Evaluation of the preservative properties of Thymus vulgaris essential oil in topically applied formulations under a challenge test. *J Appl Microbiol*. 1998 Mar;84(3):368-76. doi: 10.1046/j.1365-2672.1998.00353.x. PMID: 9721641.

15. Tabak M, Armon R, Potasman I, Neeman I. In vitro inhibition of Helicobacter pylori by extracts of thyme. *J Appl Bacteriol*. 1996 Jun;80(6):667-72. doi: 10.1111/j.1365-2672.1996.tb03272.x. PMID: 8698668.

16. Marino M, Bersani C, Comi G. Antimicrobial activity of the essential oils of Thymus vulgaris L. measured using a bioimpedometric method. *J Food Prot*. 1999 Sep;62(9):1017-23. doi: 10.4315/0362-028x-62.9.1017. PMID: 10492476.

17. Amiri H. Essential oils composition and antioxidant properties of three thymus species. *Evid Based Complement Alternat Med*. 2012;2012:728065. doi: 10.1155/2012/728065. Epub 2011 Aug 25. PMID: 21876714; PMCID: PMC3163135.

18. Van den Broucke CO, Lemli JA. Pharmacological and chemical investigation of thyme liquid extracts. *Planta Med*. 1981 Feb;41(2):129-35. doi: 10.1055/s-2007-971689. PMID: 7232550.

19. Van Den Broucke CO, Lemli JA. Spasmolytic activity of the flavonoids from Thymus vulgaris. *Pharm Weekbl Sci*. 1983 Feb 25;5(1):9-14. doi: 10.1007/BF01959645. PMID: 6844124.

20. Meister A, Bernhardt G, Christoffel V, Buschauer A. Antispasmodic activity of Thymus vulgaris extract on the isolated guinea-pig trachea: discrimination between drug and ethanol effects. *Planta Med*. 1999 Aug;65(6):512-6. doi: 10.1055/s-1999-14006. PMID: 10483369.

21. Reiter M, Brandt W. Relaxant effects on

tracheal and ileal smooth muscles of the guinea pig. *Arzneimittelforschung*. 1985;35(1A):408-14. PMID: 4039178.

22. Oliveira JR, de Jesus Viegas D, Martins APR, Carvalho CAT, Soares CP, Camargo SEA, Jorge AOC, de Oliveira LD. Thymus vulgaris L. extract has antimicrobial and anti-inflammatory effects in the absence of cytotoxicity and genotoxicity. *Arch Oral Biol.* 2017 Oct;82:271-279. doi: 10.1016/j.archoralbio.2017.06.031. Epub 2017 Jun 27. PMID: 28683409.

23. Youdim KA, Deans SG. Effect of thyme oil and thymol dietary supplementation on the antioxidant status and fatty acid composition of the ageing rat brain. *Br J Nutr.* 2000 Jan;83(1):87-93. PMID: 10703468.

24. Aeschbach R, Löliger J, Scott BC, Murcia A, Butler J, Halliwell B, Aruoma OI. Antioxidant actions of thymol, carvacrol, 6-gingerol, zingerone and hydroxytyrosol. *Food Chem Toxicol.* 1994 Jan;32(1):31-6. doi: 10.1016/0278-6915(84)90033-4. PMID: 7510659.

25. Haraguchi H, Saito T, Ishikawa H, Date H, Kataoka S, Tamura Y, Mizutani K. Antiperoxidative components in Thymus vulgaris. *Planta Med*. 1996 Jun;62(3):217-21. doi: 10.1055/s-2006-957863. PMID: 8693032.

26. Youdim KA, Deans SG. Dietary supplementation of thyme (Thymus vulgaris L.) essential oil during the lifetime of the rat: its effects on the antioxidant status in liver, kidney and heart tissues. *Mech Ageing Dev.* 1999 Sep 8;109(3):163-75. doi: 10.1016/s0047-6374(99)00033-0. PMID: 10576332.

27. Nolkemper S, Reichling J, Stintzing FC, Carle R, Schnitzler P. Antiviral effect of aqueous extracts from species of the Lamiaceae family against Herpes simplex virus type 1 and type 2 in vitro. *Planta Med*. 2006 Dec;72(15):1378-82. doi: 10.1055/s-2006-951719. Epub 2006 Nov 7. PMID: 17091431.

28. Benarba B, Gouri A. An Alternative Preventive and Therapeutic Approach to 2019-nCoV Infection. *Nat Prod Commun.* 2020;15:1934578X20944691. doi.org/10.1177/1934578X20944691

29. Gondim FL, Serra DS, Cavalcante FSÁ. Effects of Eucalyptol in respiratory system mechanics on acute lung injury after exposure to short-term cigarette smoke. *Respir Physiol Neu-*

robiol. 2019 Aug;266:33-38. doi: 10.1016/j.resp.2019.04.007. Epub 2019 Apr 28. PMID: 31022470.

30. Satyal P, Murray BL, McFeeters RL, Setzer WN. Essential Oil Characterization of Thymus vulgaris from Various Geographical Locations. *Foods*. 2016 Oct 27;5(4):70. doi: 10.3390/foods5040070. PMID: 28231164; PMCID: PMC5302419.

31. Salehi B, Mishra AP, Shukla I, Sharifi-Rad M, Contreras MDM, Segura-Carretero A, Fathi H, Nasrabadi NN, Kobarfard F, Sharifi-Rad J. Thymol, thyme, and other plant sources: Health and potential uses. *Phytother Res.* 2018 Sep;32(9):1688-1706. doi: 10.1002/ptr.6109. Epub 2018 May 22. PMID: 29785774.

32. Rizk A. The phytochemistry of the flora of Qatar, Published by King Print of Richmond. University of Qatar, Doha State. 1986.

33. Zarzuelo, A. and Crespo, E. The medicinal and non medicinal uses of thyme. In thyme. The genus Thymus. In: Stahl-Biskup, E. and Saez, F., Eds. Medicinal and Aromatic Plants Industrial Profiles, New York, Taylor and Francis. 2002; 263-292.

34. Paraskevis D, Kostaki EG, Magiorkinis G, Panayiotakopoulos G, Sourvinos G, Tsiodras S. Full-genome evolutionary analysis of the novel corona virus (2019-nCoV) rejects the hypothesis of emergence as a result of a recent recombination event. *Infect Genet Evol*. 2020 Apr;79:104212. doi: 10.1016/j.meegid.2020.104212. Epub 2020 Jan 29. PMID: 32004758; PMCID: PMC7106301.

35. Gralinski LE, Menachery VD. Return of the Coronavirus: 2019-nCoV. *Viruses.* 2020 Jan 24;12(2):135. doi: 10.3390/v12020135. PMID: 31991541; PMCID: PMC7077245.

36. Roberts A, Deming D, Paddock CD, Cheng A, Yount B, Vogel L, Herman BD, Sheahan T, Heise M, Genrich GL, Zaki SR, Baric R, Subbarao K. A mouse-adapted SARS-coronavirus causes disease and mortality in BALB/c mice. *PLoS Pathog.* 2007 Jan;3(1):e5. doi: 10.1371/journal.ppat.0030005. PMID: 17222058; PMCID: PMC1769406.

37. Pence HE, Williams A. ChemSpider: an online chemical information resource. ACS Publications, 2010.

38. BIOVIA, D.S. BIOVIA Discovery Studio Visualizer, v16. 1.0. 15350. San Diego: Dassault

Saba Hadidi.

Systèmes. 2015.

39. Neese F, Wennmohs F. ORCA (3.0. 2)- An ab initio. DFT and semiempirical SCF-MO package,(Max-Planck-Institute for Chemical Energy Conversion Stiftstr. 34-36, 45470 Mulheim ad Ruhr, Germany). 2013.

40. Berman HM, Westbrook J, Feng Z, Gilliland G, Bhat TN, Weissig H, Shindyalov IN, Bourne PE. The Protein Data Bank. *Nucleic Acids Res.* 2000 Jan 1;28(1):235-42. doi: 10.1093/nar/28.1.235. PMID: 10592235; PMCID: PMC102472.

41. Trott O, Olson AJ. AutoDock Vina: improving the speed and accuracy of docking with a new scoring function, efficient optimization, and multithreading. *J Comput Chem.* 2010 Jan 30;31(2):455-61. doi: 10.1002/jcc.21334. PMID: 19499576; PMCID: PMC3041641.

42. Laskowski RA, Swindells MB. LigPlot+: multiple ligand-protein interaction diagrams for drug discovery. *J Chem Inf Model.* 2011 Oct 24;51(10):2778-86. doi: 10.1021/ci200227u. Epub 2011 Oct 5. PMID: 21919503.

43. Gurley SB, Coffman TM. Angiotensin-converting enzyme 2 gene targeting studies in mice: mixed messages. *Exp Physiol.* 2008 May;93(5):538-42. doi: 10.1113/expphysiol.2007.040014. Epub 2008 Mar 30. PMID: 18376006.

44. Fang L, Karakiulakis G, Roth M. Are patients with hypertension and diabetes mellitus at increased risk for COVID-19 infection? *Lancet Respir Med.* 2020 Apr;8(4):e21. doi: 10.1016/S2213-2600(20)30116-8. Epub 2020 Mar 11. Erratum in: Lancet Respir Med. 2020 Jun;8(6):e54. PMID: 32171062; PMCID: PMC7118626.

45. Zhu N, Zhang D, Wang W, Li X, Yang B, Song J, et al. A Novel Coronavirus from Patients with Pneumonia in China, 2019. *N Engl J Med.* 2020 Feb 20;382(8):727-733. doi: 10.1056/NEJMoa2001017. Epub 2020 Jan 24. PMID: 31978945; PMCID: PMC7092803.

46. Bunyavanich S, Do A, Vicencio A. Nasal Gene Expression of Angiotensin-Converting Enzyme 2 in Children and Adults. *JAMA.* 2020 Jun 16;323(23):2427-2429. doi: 10.1001/jama.2020.8707. PMID: 32432657; PMCID: PMC7240631.

47. Liu M, Wang T, Zhou Y, Zhao Y, Zhang Y, Li J. Potential Role of ACE2 in Coronavirus Disease 2019 (COVID-19) Prevention and Management. *J Transl Int Med.* 2020 May 9;8(1):9-19. doi: 10.2478/jtim-2020-0003. PMID: 32435607; PMCID: PMC7227161.

48. Nejat R, Sadr AS. SARS virus papain-like protease: a mysterious weapon. Biostat. Epidemiol. 2019; 5, 288-95. doi.org/10.18502/jbe.v5i4.3873

49. Shin D, Mukherjee R, Grewe D, Bojkova D, Baek K, Bhattacharya A, et al. Papain-like protease regulates SARS-CoV-2 viral spread and innate immunity. *Nature.* 2020 Nov;587(7835):657-662. doi: 10.1038/s41586-020-2601-5. Epub 2020 Jul 29. PMID: 32726803; PMCID: PMC7116779.

50. McClain CB, Vabret N. SARS-CoV-2: the many pros of targeting PLpro. *Signal Transduct Target Ther.* 2020 Oct 6;5(1):223. doi: 10.1038/s41392-020-00335-z. PMID: 33024071; PMCID: PMC7537779.

51. Zhang L, Lin D, Sun X, Curth U, Drosten C, Sauerhering L, et al. Crystal structure of SARS-CoV-2 main protease provides a basis for design of improved α-ketoamide inhibitors. *Science.* 2020 Apr 24;368(6489):409-412. doi: 10.1126/science.abb3405. Epub 2020 Mar 20. PMID: 32198291; PMCID: PMC7164518.

52. Jin Z, Du X, Xu Y, Deng Y, Liu M, Zhao Y, et al. Structure of Mpro from SARS-CoV-2 and discovery of its inhibitors. *Nature.* 2020 Jun;582(7811):289-293. doi: 10.1038/s41586-020-2223-y. Epub 2020 Apr 9. PMID: 32272481.

53. Kaysser L. Built to bind: biosynthetic strategies for the formation of small-molecule protease inhibitors. *Nat Prod Rep.* 2019 Dec 11;36(12):1654-1686. doi: 10.1039/c8np00095f. PMID: 30976762.